
Article:
Rajashekhar, A., Zhang, H-R., Srowthi, B. et al. (2 more authors) (2016) Microstructure Evolution of In Situ Pulsed-Laser Crystallized Pb(Zr0.52Ti0.48)O3 Thin Films. Journal of the American Ceramic Society, 99 (1). pp. 43-50. ISSN 0002-7820

https://doi.org/10.1111/jace.13944

Microstructure Evolution of In Situ Pulsed-Laser Crystallized $Pb(Zr_{0.52}Ti_{0.48})O_3$ Thin Films

A. Rajashekhar[1], H. R. Zhang[3], S. S. N. Bharadwaja[2], I. M. Reaney[3] and

S. Trolier-McKinstry[1,2]

[1]Department of Materials Science and Engineering, Pennsylvania State University, University Park, PA-16802, USA

Fax: 1-814-865-7173, e-mail: adarshr@psu.edu

[2]Materials Research Institute, Pennsylvania State University, University Park, PA-16802, USA

[3]Department of Materials Science and Engineering, University of Sheffield, Sheffield, S1 3JD, UK

Abstract

Integration of lead zirconate titanate (PZT) films with temperature sensitive substrates (CMOS, polymers) would benefit from growth at substrate temperatures below 400˚C. In this work, in situ pulsed-laser annealing[1] was used to grow crystalline lead zirconate titanate ($PbZr_{0.52}Ti_{0.48}O_3$) thin films at a substrate temperature of ~370˚C on $PbZr_{0.30}Ti_{0.70}O_3$-buffered platinized silicon substrates. Transmission electron microscopy (TEM) analysis indicated that the films were well crystallized into columnar grains, but with pores segregated at the grain boundaries. Lateral densification of the grain columns was significantly improved by reducing the partial pressure of oxygen from 120 mTorr to 50 mTorr, presumably due to enhanced adatom mobility at the surface accompanying increased bombardment. It was found that varying the fractional annealing duration with respect to the deposition duration produced little effect on lateral grain growth. However, increasing the fractional annealing duration led to shift of 111 PZT X-ray

diffraction peaks to higher 2θ values, suggesting residual in-plane tensile stresses in the films. Thermal simulations were used to understand the annealing process. Evolution of the film microstructure is described in terms of transient heating from the pulsed laser determining the nucleation events, while the energy of the arriving species dictates grain growth/coarsening.

I. Introduction

Piezoelectric PZT thin films are being increasingly utilized in micro-electromechanical systems (MEMS) as micro-actuators, sensors and transducers. However, fabrication of these MEMS structures generally requires the active piezoelectric element to be physically separated from the read-out or driving circuits. This necessity arises since processing temperatures for PZT (> 550˚C) are significantly higher than those tolerated by most completed complementary metal oxide semiconductor (CMOS) circuits (< ~425˚C)[2,3]. On the other hand, direct integration of the piezoelectric thin film with a microchip would improve response times in sensors, potentially coupled with low-cost manufacturing[4]. Pulsed-laser treatment is one way to selectively heat the film to achieve the high temperatures required for perovskite phase crystallization, while causing minimal heating of the underlying substrate[5,6,7,8,9,10,11].

Moreover, in situ heat treatment of oxide thin films during growth can also benefit from reduced crystallization temperatures compared to a post-deposition thermal processing[12,13]. It has been shown that crystallization of ferroelectric thin films can be achieved by simultaneous laser annealing during growth at substrate temperatures of $\leq 400°C$[1,14,15]. This approach also eliminates film thickness constraints due to limited thermal penetration depth of the absorbed laser pulse. Selected orientations can also be achieved by controlling nucleation from the substrate. It was demonstrated that oriented perovskite $PbZr_{0.52}Ti_{0.48}O_3$ (PZT(52/48)) thin films with a thickness of the order of a micron[1] could be grown using this technique. The film microstructure was characterized by fine columnar grains caused by a large nucleation density.

The functional properties of PZT thin films are heavily dependent on the crystallization as well as the microstructure. Hence it becomes imperative to understand the effect of growth parameters and pulsed laser heating on the evolution of the microstructure in PZT thin films produced by this technique. This

paper describes the microstructures of the thin films grown by in situ laser annealing along with the mechanisms responsible for the microstructure development.

II. Experimental Procedure

A pulsed laser deposition (PLD) system with in situ laser annealing as described in Ref.[1] was used in this work. A single 248 nm KrF excimer laser with a 20 ns pulse-width and 20 Hz repetition rate was used for PLD as well as the annealing, where a 50-50 beam splitter was utilized to carry out the two functions simultaneously. Figure 1 depicts the geometry of the substrate holder with respect to the ablation plume and annealing beam. The center of the annealing spot is offset from the substrate rotation axis, and as a result, the growing film spent only a fraction of time per rotation in the deposition plume or the annealing beam.

As in Ref.[1], growth with a seed-layer was adopted in this work. A low temperature seed-layer (by ex situ laser annealing) was demonstrated in[1], where it was seen that growth on laser-crystallized and rapid thermally annealed (RTA'd) seed-layers yielded comparable highly columnar growth, and well crystallized films. As the aim of this work was to study the growth mechanism associated with in situ laser annealing, the crystallization temperature of the seed-layer was not critical for the current experiments. Hence, a sol-gel[16] $PbZr_{0.30}Ti_{0.70}O_3$ (PZT(30/70)) seed-layer on (111)Pt/Ti/SiO_2/Si wafers (from Nova Inc.), RTA furnace crystallized at 700˚C for 1 min was used as the substrate. A PZT(52/48) PLD target with 20%-excess PbO prepared by a conventional solid-state mixed oxide route was utilized for ablation in the laser fluence range of 1 – 2 J/cm^2. The target-substrate distance studied was in the range of 5 – 7.2 cm while the substrate temperature used was maintained around ~350 – 380 ˚C to provide some additional thermal energy. The laser annealing energy densities lay between 50 and 60 mJ/cm^2. A 90% oxygen/10% ozone ambient was utilized at chamber pressures between 50 – 120 mTorr. The substrate was rotated at 10 rpm to increase the annealing area. After the final ablation pulse was

completed, the annealing pulses were continued for an additional 60 seconds, so as to crystallize any surface layers deposited by the last ablation pulses.

Phase-formation and orientation of the films were characterized by X-ray diffraction (XRD) using Cu-Kα radiation from a Philips Analytical X-ray diffractometer (PANalytical XPert Pro MPD). Microstructural studies were carried out using a Leo 1530 field emission scanning electron microscope (FE-SEM) and a JEOL 2010F scanning transmission electron microscope (STEM/TEM) equipped with a high angle annular dark-field (HAADF) detector and an Oxford Instruments energy dispersive X-ray spectroscopy (EDS) system and Gatan Image Filter (GIF) system. Compositional uniformity measurements were performed by EDS in STEM mode with an electron probe of 1 nm diameter.

Optical characterization was carried out at room temperature using a rotating compensator spectroscopic ellipsometer (M-2000; J. A. Woollam Co.) at three angles of incidence (θ_i = 55˚, 65˚ and 75˚) and over the spectral range of 500 nm to 1690 nm; CompleteEASE software was used to fit the data. For electrical characterization, circular top electrodes (75 – 200 μm diameter) were defined by optical lithography; 100 nm of Pt was deposited using a Kurt J. Lesker sputtering tool and patterned by lift-off. The top electrodes were annealed at 375˚C for 2 minutes in an RTA furnace. A multiferroic tester from Radiant Technologies was used to perform the polarization-electric field (P-E) hysteresis measurements at 100 Hz. Photothermal heating due to a single laser pulse was modeled using the finite element method (similar to in Ref.[17]) in COMSOL 5.0 Multiphysics software. Material properties were taken from Ref.[7,18].

III. Results and Discussion

Crystallization

TEM analysis was carried out on an in situ laser annealed PZT(52/48) film (~350 nm thick) deposited at an ablation fluence of ~1.8 J/cm^2, with a target-substrate distance of 7.2 cm, at a pO_2 of 70 mTorr, an

annealing energy density ~55 mJ/cm^2 and on a sol-gel crystallized PZT(30/70) seed-layer (~70 nm thick). A multi-beam dark-field TEM image taken with several Bragg diffraction beams shows that the film is columnar (Figure 2(a)). Figure 2(b) (inset) shows a [111] zone-axis electron diffraction pattern (EDP) taken from a single column. Further EDPs revealed that each column was a single grain. The mottled contrast in the single grain in the diffraction contrast image of Figure 2(a) may arise because local defects and compositional variations reduce the size of ferroelectric domains and disrupt the habit planes of their walls. Note that the seed-layer (Zr:Ti ratio 30:70) contains planar domain walls typical of a tetragonal ferroelectric. In this instance, the larger spontaneous strain with respect to the bulk of the film (Zr:Ti ratio 52:48) forces longer range polar coupling despite a similar density of local defects. High resolution TEM (not shown here) revealed local epitaxy across the seed-layer – film interface. However, layers of pores were found to be segregated at the grain boundaries, as can be seen in the STEM bright-field image (Figure 2(b)).

Microstructure Development

It is important to consider what determines the film densification. Atomistically, surface and bulk diffusion are expected to play a role in determining the microstructure in any thin film growth process. Here, the diffusivities are primarily a function of the energy of the arriving vapor species as well as the pulsed-laser heating. To assess these independently, the energy of the incident atoms was varied via the gas pressure in the chamber. Figure 3 and Figure 4 show the microstructures of films deposited at chamber pressures between 50 mTorr and 120 mTorr. For these experiments, the ablation-fluence (~1.7 J/cm^2), the annealing energy-density (~55 mJ/cm^2), and the target-substrate distance (6 cm) were held constant. A ~50nm thick PZT(30/70) seed layer was used. Higher pressures imply more scattering of the plume species with the ambient gas molecules, effectively reducing the energy of the atoms/ions arriving at the substrate[19]. It was found that this produces a less dense, fine grained structure, with pores visible along the grain boundaries (120 mTorr). Reducing the O_2 pressure to 70 mTorr acts to densify the film, but the fine-grained structure is maintained, with some remanent porosity. At chamber pressures of 50

mTorr, coarsening of the fine grains (to ~200 nm diameter), with concomitant densification is observed. The improvement in crystallinity (inferred from the cross-sectional SEM and sharp peaks in the XRD pattern) may also be due to the higher energy of the depositing species associated with reduced collisions between the plume species and the chamber gas at low pO_2. Micro-cracking, which points to growth-induced residual stresses, was also observed.

Increased bombardment contributes to densification by forward scattering of the surface atoms; films deposited under high bombardment conditions also show lower surface roughnesses[20]. However, excessive bombardment may induce Pb re-sputtering. Reducing the target-substrate distance to 5 cm, while maintaining the pressure at 50 mTorr, achieved similar densification, but with increased Pb loss from re-sputtering giving rise to some lead-deficient pyrochlore/fluorite phase (Figure S 1, XRD shown in Figure S 2 of Supplemental Information).

To compare the properties to conventional films, the refractive indices of the film deposited at 50 mTorr and 6 cm target-substrate distance were extracted from spectroscopic ellipsometry in the wavelength range of 500 nm to 1690 nm. A model consisting of roughness/PZT(52/48)/PZT(30/70)/Pt was used for this purpose (Figure S 3(d), Supplemental Information). Since PZT is transparent in this spectral range, Sellmeier models[21] were utilized to model the optical constants for both PZT(52/48) as well as PZT(30/70). The model fits for the spectroscopic ellipsometry parameters of Psi (ψ) and Delta (Δ) (with a weighted root Mean Squared Error (MSE)[22] of 14.5) are shown in Figure S 3(a) and (b) (Supplemental Info). The refractive index obtained was compared with those for the same composition film (PZT(52/48)) reported in Ref.[23] (Figure S 3(c)). The difference in the refractive index was seen to arise from a porosity level of ~2.7 volume% as obtained from a Bruggeman effective medium model.

STEM-EDS line scan analysis was carried out on the sample deposited at a pO_2 of 50 mTorr and 6 cm target-substrate distance to study compositional homogeneity, as illustrated in Figure 5(a). A vertical EDS scan demonstrates that the film is compositionally uniform through most of the thickness (Figure 5(b)).

However, the Pb concentration near the film – seed-layer interface is enhanced relative to the rest of the film; the reason for this is currently unknown. No significant compositional heterogeneity was observed across the grain boundary (Figure 5(c)). The HAADF image (Figure 5(d)) corroborates the large grain size witnessed in the cross-sectional FE-SEM, and also shows some trapped layered porosity within the grains as expected from the spectroscopic ellipsometry.

Laser annealing duration as a fraction of the deposition time was also varied to understand the role of laser-induced diffusion, while maintaining other factors constant at an ablation fluence ~1.7 J/cm^2, annealing energy density: ~55 mJ/cm^2, target-substrate distance: 6 cm, pO_2: 85 mTorr, and deposition duration: 1.5 hours. To achieve this, an electronic shutter (SmartShutter® from Sutter Instrument Company, controlled using a Lambda SC control unit) was used on the annealing arm of the laser pathway. The 'fractional anneal time' (f_t^{Anneal}) was defined as the ratio of the annealing duration to the total ablation (deposition) duration. With the shutter for annealing continuously open, the total durations for annealing and deposition are the same, hence giving an f_t^{Anneal}=1. The ratio of the pulses was maintained continuously in real time to minimize any spatial variation as the substrate was rotated. Consider, for example, the case of f_t^{Anneal} of 0.27 (= 3/11). Here, a single shutter open/close cycle consisted of 11 consecutive annealing (and ablation) laser pulses, with a laser repetition rate of 20 Hz. Of these only a set of 3 annealing pulses were let in, while the subsequent 8 pulses on the annealing arm were blocked). For all the cases investigated (listed in Table I), the annealing shutter open duration (packets of 3 annealing pulses at a time) was kept constant, while the shutter close time was varied (the number of annealing pulses let in plus the number of blocked annealing pulses give the total number of deposition pulses per cycle). This was done while maintaining a constant total deposition time. The approximate numbers of cumulative annealing pulses seen by the sample were calculated for each f_t^{Anneal} using the substrate rotation geometry and are listed in Table I. The approximate growth rate was also estimated as ~0.3 Å/pulse for all cases.

The X-ray diffraction patterns of the films (~590 nm thick PZT(52/48) on ~50 nm PZT(30/70) sol-gel seed) along with that of a film that saw no laser annealing and the PZT(30/70) seed-layer are shown in Figure 6. The film which was not laser-annealed primarily showed the pyrochlore phase along with seed-layer and substrate peaks. The films with different fractional anneals are all crystalline but with varying degrees of preferred orientation. Figure 7(a), (b) and (c) show the 111_{pc}, 110_{pc} and 100_{pc} (pc: pseudocubic perovskite) PZT peaks for the films. These peaks were fit to Lorentzian profiles using Mathematica® and integrated peak-intensities, peak-positions, and full-width-at-half-maxima(FWHM) were extracted. As shown in Figure 7(d), on increasing thef_t^{Anneal}, an increase in the integrated-intensity of the 111_{pc} PZT(52/48) peak is seen along with a corresponding reduction in the integrated-intensities of the 110_{pc} and 100_{pc} peaks. That is, smaller laser f_t^{Anneal} promote a more random orientation. One possibility is that the random orientation with low f_t^{Anneal} is characteristic of grains nucleating from a pyrochlore matrix[24]. With higher f_t^{Anneal}, 111_{pc} orientation is preferred, presumably as a result of preferential nucleation from the substrate. Alternatively, it is possible that in the initial stages of the film growth, grains with 111_{pc} orientation outgrow the ones oriented along the 100_{pc} and 110_{pc} directions on increasing f_t^{Anneal}, hence yielding the current trend. A concomitant shift of the 111_{pc} peak to higher 2θ angles is also seen (Figure **7**(e)) with increasing f_t^{Anneal}. If these shifts are entirely due to the development of an in-plane residual tensile strain, a consequent out-of-plane compressive strain of about -0.5% can be inferred on going from an f_t^{Anneal}=0.09 to an f_t^{Anneal}=1. It should be noted that neither the seed-layer 111 peak nor the 111 Pt peak are affected, indicating that the peak shift is induced by the in situ laser annealing growth process of PZT(52/48). However, the origin of a corresponding increase in the FWHM of the 111_{pc} peaks with increasing f_t^{Anneal} is currently not understood. Nested polarization-electric field hysteresis loops and leakage currents at 3 times the coercive field are shown in supplemental information Figure S 5 and the corresponding remanent polarization (P_r) and coercive field (E_c) values are also listed in Table S 2. The microstructural changes accompanying the increased f_t^{Anneal} are shown in Figure 8. It

is important to note that all the films show fine-grained columnar microstructures which are maintained with increased f_t^{Anneal}. Lateral growth or coarsening of the grains is not observed. Micro-voids become apparent on the surface when the film is subjected to an f_t^{Anneal} of 0.3 (Figure 8(f)), while micro-cracks are observed in the cases of 0.5 and 1 (Figure 8(h) & (j)). The microcracking is likely to be the result of the in-plane tensile stresses.

It is clear that a cumulative number of laser pulses of less than ~1200 (f_t^{Anneal}= ~0.09) can crystallize a ~590 nm thick PZT(52/48) on a PZT(30/70) seed layer. In comparison, in Ref.[25], 320-350 nm thick PZT(52/48) films were crystallized on a $PbTiO_3$ seed layer at 375˚C substrate temperature using about 4800-6000 pulses (using an energy density of 40-45 mJ/cm^2). Here, for an equivalent thickness, only about 650-712 pulses would have been needed at f_t^{Anneal}= ~0.09. In this case, every 33 deposition pulses (correspond to ~10 Å with respect to the growth rate) get 3 annealing pulses (which yields ~3.3 Å per annealing pulse). Simulations of the temperature profiles (explained in supplemental information) due to photothermal heating by a single laser-pulse (with fluence = 55 mJ/cm^2 and pulsewidth = 20 ns, substrate temperature = 350˚C) at various depths in a 300 nm thick PZT (e.g.,) on Pt/Ti/SiO_2/Si substrate (Figure 9), show that the surface layers experience extremely high thermal excursions (T_{max} of ~1400˚C). Temperatures exceeding 600˚C are maintained for about 161 ns per pulse at the surface and are realized to a depth of ~250 nm inside the PZT. This suggests that each annealing pulse can potentially influence the crystallization to a comparatively large depth.

The thermal profiles are also compared to that of 100 nm and 600 nm thick PZT (Figure S 4, Supplemental Information). It can be seen that although surface temperatures achieved for a 600 nm film are comparable to that of the 300 nm film (~1410˚C), temperatures over 600˚C are achieved only to a depth of ~300 nm in this case. Thus, a film of this thickness cannot be ex situ laser crystallized through the entire thickness with the given conditions. Instead, a sequential growth and crystallization route is necessary. For the 100 nm film, however, the surface temperatures achieved are lower (~1263˚C),

although the entire PZT film thickness experiences maximum temperatures higher than 600˚C. It should be noted that in all of these cases, the SiO_2/Si interface experiences low thermal budgets (T_{max} ~370˚C).

The structure zone model (SZM) was developed to describe the film microstructures characteristic of physical vapor deposition processes[26,27]. The observed microstructure is a function of the homologous temperature, T_h (= T_s/T_m; where T_s: substrate temperature, T_m: melting point) and varies from Zone I (at low T_h; characterized by a low density structure and fine fiber texture due to very low adatom mobility) through Zone T (slightly higher T_h; characterized by a columnar structure, but immobile grain boundaries, with limited surface mobility sufficient for local epitaxy on top of a grain) to Zone II (high T_h regime where significant bulk diffusion operates giving rise to grain boundary migration and grain coarsening).

The microstructures of PZT films with varying f_t^{Anneal}indicate that pulsed laser heating primarily produces structures which lie in between Zone I and Zone T, which is surprising given the high surface temperatures seen as a result of pulsed laser irradiation. It is believed that a high density of nuclei is responsible for the observation of such fine grain features irrespective of the f_t^{Anneal} values. In this case, the activation barrier for nucleation of the perovskite phase is low due to a high thermodynamic driving force for crystallization (ΔG_v), which is the difference between the free energy of the crystalline solid and the metastable amorphous/pyrochlore deposited material at the low substrate temperature[28,29] (Figure S 6, Supplemental Information). This gives rise to a high nucleation rate[30,31]. Furthermore, the larger this driving force is, the smaller the size of critical nuclei that should be required. In the case of laser ablation with simultaneous annealing at 20 Hz, the film sees an annealing laser pulse and a vapor pulse every 50 ms. Simulations of the laser-induced heat-pulse suggests a decay to the background (substrate) temperature on the order of a few microseconds (Figure 9). Thus, the effective time at temperatures high enough for bulk diffusion is quite short. Furthermore, the lateral growth rates, determined by an activation energy that is independent of the driving force for crystallization[32], are low compared to the nucleation rates. Consequently, although the laser pulses provide the bursts of energy required for short-range diffusion such that the crystallization reaction can occur, long-range diffusion is kinetically limited.

Moreover, the adatom mobility is low between consecutive ablation/annealing pulses (in contrast to conventional PLD where high substrate temperatures enable nuclei to undergo ripening in between pulses[33]). It is believed that these factors account for the observed Zone I/Zone T structures.

With respect to the growth stresses, it is reported in the literature on metal thin films that the coalescence of grains to form grain boundaries produces a residual tensile stress[34]. This tensile stress increases with decreasing grain size and is accentuated by low adatom mobility conditions[34,26]. Another model for the generation of tensile stress[35] is the constrained shrinkage that occurs during annealing of disordered material beneath the surface, while the film is being coated further with an incoming flux. The volume reduction associated with the amorphous/pyrochlore/perovskite transformation in PZT[36,37] could potentially give rise to shrinkage-induced stresses. However, this mechanism for stress development would be more prominent at lower f_t^{Anneal} since, on average, a larger thickness of the film that needs to be crystallized is accumulated in between the annealing pulses. This in turn would mean larger tensile stresses at smaller f_t^{Anneal}, which is opposite to the observed trend. In addition, for PZT and other Pb-containing oxides, any unreacted excess PbO can micro-segregate at the grain boundaries and subsequently evaporate on experiencing high temperatures during laser heat treatment. A combination of one or more of these factors could give rise to an intrinsic tensile stress and/or prevent complete coalescence of the grains, leaving pores.

IV. Conclusions

Simultaneous pulsed-laser heating during growth was utilized to crystallize PZT(52/48) thin films on PZT(30/70) seeded platinized-silicon substrates at a substrate-temperature of ~370 ˚C. Crystalline films were produced, but TEM measurements showed porosity segregated at the grain boundaries under some conditions. It was demonstrated that the energy of the plume species played a dominant role in lateral densification and in affecting the grain sizes. Energy dispersive spectroscopy measurements showed that films were chemically homogeneous with no significant non-uniformity at the grain boundaries. The fine-

grained columnar microstructure is preserved on varying the fractional laser annealing times, suggesting that nucleation and growth occurs in the direction normal to the substrate, with little or no lateral growth/densification due to laser annealing pulses.

V. Acknowledgements

This research is funded by the National Security Science, Engineering Faculty Fellowship (NSSEFF) from the Office of the Secretary of Defense (DoD) and the Engineering and Physical Sciences Research Council (EP/I038934/1), United Kingdom. The author would like to thank Charles Yeager and Margeaux Wallace for providing with the sol-gel films used in this work. The author is also grateful to Albert Queralto for assisting with the thermal simulations in COMSOL.

VI. References

[1] A. Rajashekhar, A. Fox, S.S.N. Bharadwaja, and S. Trolier-McKinstry, "In situ Laser Annealing During Growth of $Pb(Zr_{0.52}Ti_{0.48})O_3$ Thin Films," Appl. Phys. Lett., **103** [3] 032908 (2013).

[2] R.W. Whatmore, P.B. Kirby, A. Patel, N.M. Shorrocks, T. Bland, and M. Walker, "Ferroelectric Thin Films for Capacitor and Sensor Applications;" pp. 383–397 in Proc. NATO Adv. Res. Work. Sci. Technol. Electroceramic Thin Film. 1994.

[3] H. Takeuchi, A. Wung, X. Sun, R.T. Howe, and K. Tsu-Jae, "Thermal Budget Limits of Quarter-Micrometer Foundry CMOS For Post-Processing MEMS Devices," IEEE Trans. Electron Devices, **52** [9] 2081–2086 (2005).

[4] G.K. Fedder, R.T. Howe, T.-J. King Liu, and E.P. Quevy, "Technologies for Cofabricating MEMS and Electronics," Proc. IEEE, **96** [2] 306–322 (2008).

[5] X.M. Lu, J.S. Zhu, X.F. Huang, C.Y. Lin, and Y.N. Wang, "Laser-Induced Phase Transformation from Amorphous to Perovskite in $PbZr_{0.44}Ti_{0.56}O_3$ Films with the Substrate at Room Temperature," Appl. Phys. Lett., **65** [16] 2015–2017 (1994).

[6] Y. Zhu, J. Zhu, Y.J. Song, and S.B. Desu, "Laser-assisted low temperature processing of PZT thin films," Mater. Res. Soc. Symp. Proc., **493** 305–309 (1998).

[7] S. Bharadwaja, J. Kulik, R. Akarapu, H. Beratan, and S. Trolier-McKinstry, "Ultrafast Crystallization Kinetics in $(Pb, La)(Zr_{0.30}Ti_{0.70})O_3$ Thin Films by Pulsed Excimer Laser Annealing," IEEE Trans. Ultrason. Ferroelectr. Freq. Control, **57** [10] 2182–2191 (2010).

[8] S.S.N. Bharadwaja, T. Dechakupt, S. Trolier-McKinstry, and H. Beratan, "Excimer Laser Crystallized (Pb,La)(Zr,Ti)O_3 Thin Films," J. Am. Ceram. Soc., **91** [5] 1580–1585 (2008).

[9] T. Nakajima, T. Tsuchiya, M. Ichihara, H. Nagai, and T. Kumagai, "Epitaxial Growth Mechanism for Perovskite Oxide Thin Films under Pulsed Laser Irradiation in Chemical Solution Deposition Process," Chem. Mater., **20** 7344–7351 (2008).

[10] O. Baldus and R. Waser, "Experimental and Numerical Investigations of Heat Transport and Crystallization Kinetics in Laser-induced Modification of Barium Strontium Titanate Thin Films," Appl. Phys. A, **80** [7] 1553–1562 (2004).

[11] T. Miyazaki, S. Sou, N. Sakamoto, N. Wakiya, and H. Suzuki, "Low-Temperature Crystallization of CSD-derived PZT Thin Film with Laser Assisted Annealing," J. Ceram. Soc. Japan, **173** [1-3] 950–953 (2009).

[12] R. Roy and K. Etzold, "Substrate and Temperature Effects in Lead Zirconate Titanate Films Produced by Facing Targets Sputtering," J. Mater. Res., **7** [6] 1455–1464 (1992).

[13] J.S. Horwitz, K.S. Grabowski, D.B. Chrisey, and R.E. Leuchtner, "In Situ Deposition of Epitaxial $PbZr_xTi_{(1-x)}O_3$ Thin Films by Pulsed Laser Deposition," Appl. Phys. Lett., **59** [13] 1565–1567 (1991).

[14] H. Tabata, T. Kawai, S. Kawai, O. Murata, J. Fujioka, and S. Minakata, "Preparation of $PbTiO_3$ Thin Films at Low Temperature by an Excimer Laser Ablation Technique," Appl. Phys. Lett., **59** [19] 2354 (1991).

[15] H. Tabata, O. Murata, T. Kawai, S. Kawai, and M. Okuyama, "Preparation of $PbTiO_3$ Thin Films by an Excimer Laser Ablation Technique with Second Laser Irradiation," Jpn. J. Appl. Phys., (1992).

[16] K.D. Budd, S.K. Dey, and D.A. Payne, "Sol-Gel Processing of $PbTiO_3$, $PbZrO_3$, PZT and PLZT Thin Films," Br. Ceram. Proc., **36** pp. 107–121 (1985).

[17] A. Queraltó, A. Pérez del Pino, M. de la Mata, J. Arbiol, X. Obradors, and T. Puig, "Ultrafast Crystallization of $Ce_{0.9}Zr_{0.1}O_{2-y}$ Epitaxial Films on Flexible Technical Substrates by Pulsed Laser Irradiation of Chemical Solution Derived Precursor Layers," Cryst. Growth Des., **15** [4] 1957–1967 (2015).

[18] [Online], Material Property Data, www.matweb.com, (n.d.).

[19] D.B. Geohegan, "Diagnostics and Characterization of Pulsed Laser Deposition Laser Plasmas;" pp. 115–165 in Pulsed Laser Depos. Thin Film. Edited by D.B. Chrisey and G.K. Hubler. John Wiley & Sons, 1994.

[20] D.L. Smith, "Surface Effects;" pp. 402–411 in Thin-Film Depos. Princ. Pract. McGraw-Hill, 1995.

[21] H. Fujiwara, "Dielectric Function Models;" pp. 158–176 in Spectrosc. Ellipsom. Princ. Appl. John Wiley & Sons, 2007.

[22] B.D. Johs, R.H. French, F.D. Kalk, W.A. McGahan, and J.A. Woollam, Optical Analysis of Complex Multilayer Structures Using Multiple Data Types, SPIE Proceedings, Opt. Interf. Coatings, **2253** 1098–1106 (1994).

[23] S. Trolier-McKinstry, H. Hu, S. Krupanidhi, P. Chindaudom, K. Vedam, and R. Newnham, "Spectroscopic Ellipsometry Studies on Ion Beam Sputter Deposited Pb(Zr, Ti)O_3 Films on Sapphire and Pt-Coated Silicon Substrates," Thin Solid Films, **230** 15–27 (1993).

[24] I. Reaney, D. Taylor, and K. Brooks, "Ferroelectric PZT Thin Films by Sol-Gel Deposition," J. Sol-Gel Sci. Technol., **13** 813–820 (1998).

[25] S.S.N. Bharadwaja, F. Griggio, J. Kulik, and S. Trolier-McKinstry, "Highly textured laser annealed Pb($Zr_{0.52}Ti_{0.48}$)O_3 thin films," Appl. Phys. Lett., **99** [4] 042903 (2011).

[26] J. Thornton, "High Rate Thick Film Growth," Annu. Rev. Mater. Sci., **7** 239–260 (1977).

[27] I. Petrov, P.B. Barna, L. Hultman, and J.E. Greene, "Microstructural Evolution During Film Growth," J. Vac. Sci. Technol. A Vacuum, Surfaces, Film., **21** [5] S117 (2003).

[28] R.W. Schwartz, "Chemical Solution Deposition of Perovskite Thin Films," Chem. Mater., **9** [97] 2325–2340 (1997).

[29] R. Roy, "Gel Route to Homogeneous Glass Preparation," J. Am. Ceram. Soc., **52** [6] 344 (1969).

[30] M. Ohring, "Nucleation Dependence on Substrate Temperature and Deposition Rate;" pp. 383–386 in Mater. Sci. Thin Film. Depos. Struct. Academic Press, 2001.

[31] D.L. Smith, "Three-Dimensional (3D) Nucleation;" pp. 145–154 in Thin Film Depos. Princ. Pract. McGraw-Hill, 1995.

[32] J.W. Christian, The Theory of Transformations in Metals and Alloys (Part I and II). 2002.

[33] D.B. Chrisey and G.K. Hubler, Pulsed Laser Deposition of Thin Films. Wiley Interscience, 1994.

[34] W. Nix and B. Clemens, "Crystallite Coalescence- A Mechanism for Intrinsic Tensile Stresses in Thin Films," J. Mater. Res., **14** [8] 3467–3473 (1999).

[35] E. Klokholm and B.S. Berry, "Intrinsic Stress in Evaporated Metal Films," J. Electrochem. Soc., **115** [8] 823–826 (1968).

[36] S. Corkovic, Q. Zhang, and R.W. Whatmore, "The Investigation of Key Processing Parameters in Fabrication of Pb(Zr_xTi_{1-x})O_3 Thick Films for MEMS Applications," J. Electroceramics, **19** [4] 295–301 (2007).

[37] C. Kwok and S. Desu, "Pyrochlore to Perovskite Phase Transformation in Sol-Gel Derived Lead-Zirconate-Titanate Thin Films," Appl. Phys. Lett., **60** [12] 1430–1432 (1992).

List of Figures

Figure 9: Temperature evolution at different depths inside 300 nm PZT on Pt/Ti/SiO_2/Si substrate. The laser pulse profile is also shown.

List of Tables

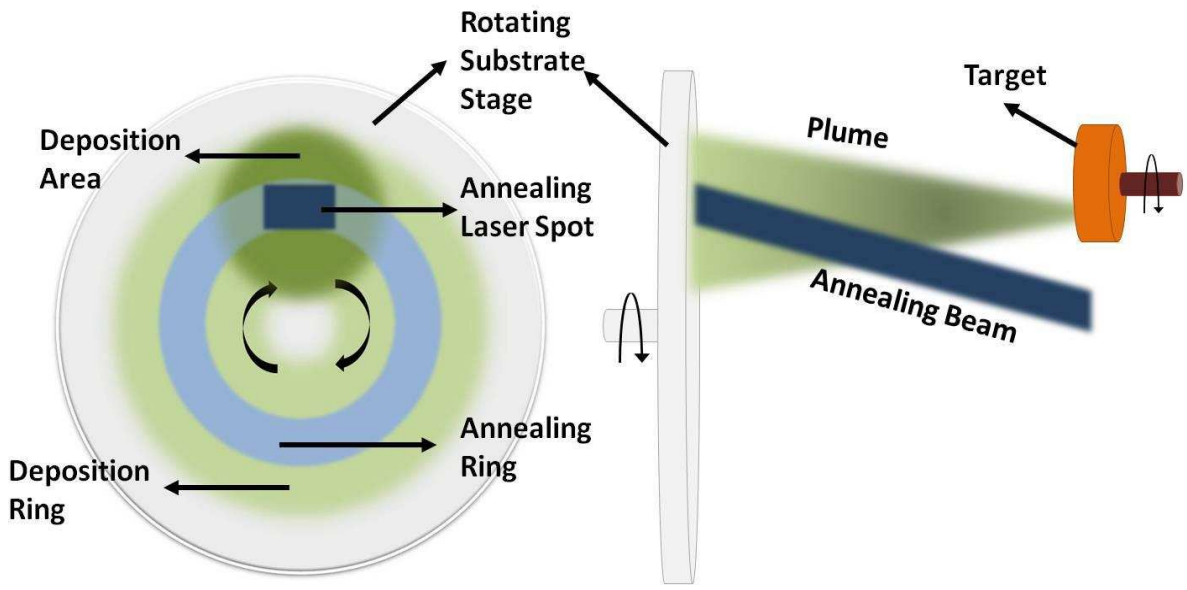

Figure 1: Schematic of the laser annealing process during growth by PLD. The annealing beam was ~1.6 cm X ~0.8 cm while the center of the annealing beam was located ~2cm above the center of the holder. The extent of the deposition vapor on the substrate holder was ~2.5 cm. The substrate was rotated at 10 rpm.

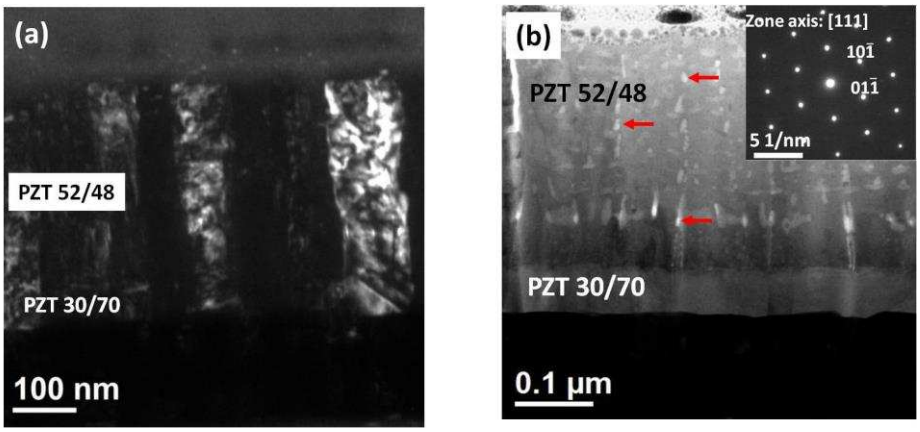

Figure 2: (a) Multi-beam dark-field TEM image of in situ annealed PZT film (b) STEM bright-field image showing pore segregation at the grain boundaries (some marked with red arrows). Inset in (b) shows the selected area electron diffraction pattern of a column showing good crystallinity of the grain.

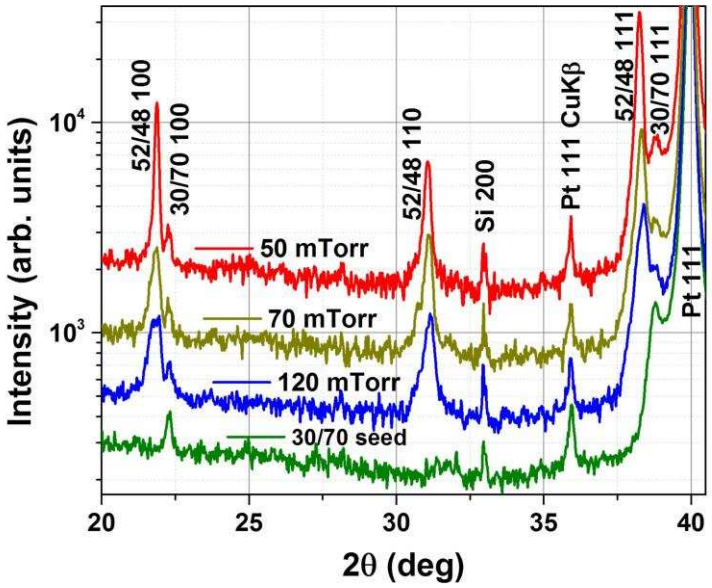

Figure 3: XRD of films deposited at various pO_2 chamber pressures. The XRD of the PZT(30/70) seed-layer is included for comparison. The ablation-fluence was ~1.7 J/cm^2, laser annealing energy-density was ~55 mJ/cm^2 and the target-substrate distance was 6 cm.

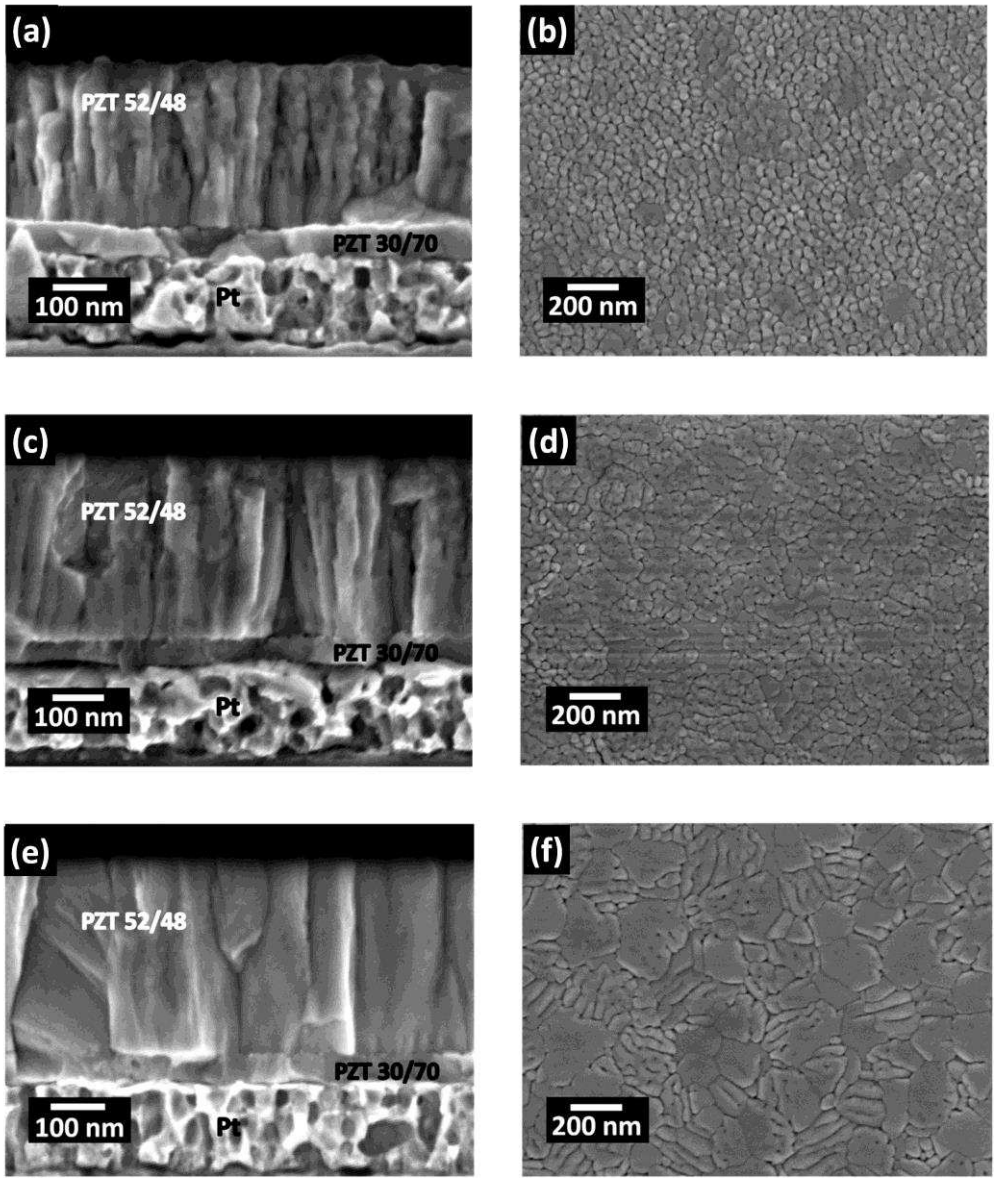

Figure 4: Cross-sectional and plan-view FESEM of PZT films deposited at different pO_2; (a) & (b) 120 mTorr, (c) and (d) 70 mTorr, (e) and (f) 50 mTorr

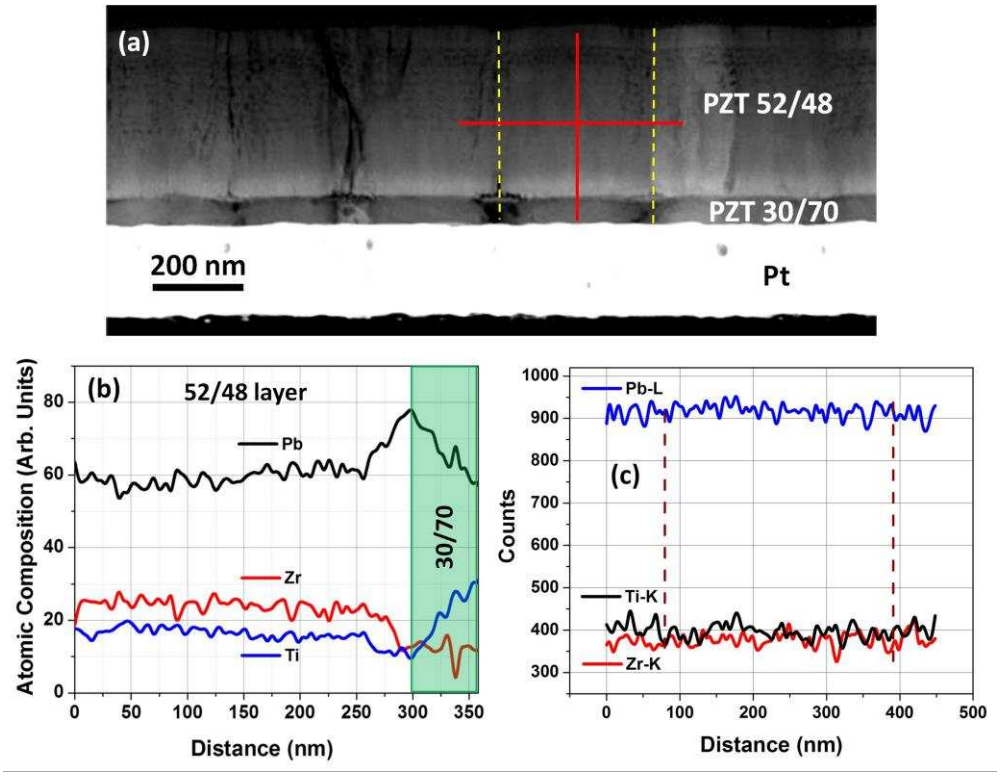

Figure 5: (a) an HAADF image showing large grain sizes and some layered porosity. The vertical and horizontal lines along which EDS scans were carried out are marked (red lines); The dashed vertical lines denote the positions of the grain boundaries, (b) vertical EDS and (c) horizontal EDS scan intensities of Pb-L, Zr-K and Ti-K peaks

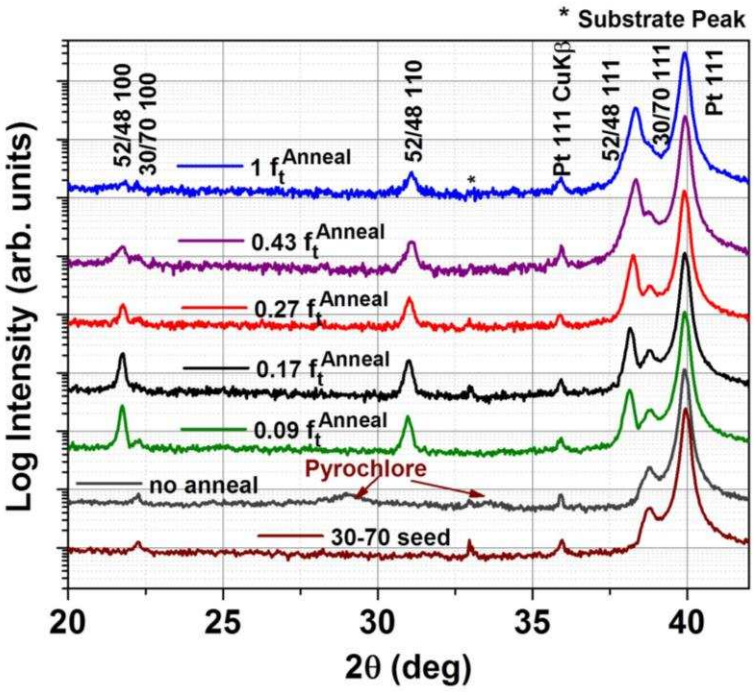

Figure 6: Evolution of crystallization with different fractional laser anneal times. The peak position marked with an asterisk (*) is from the substrate.

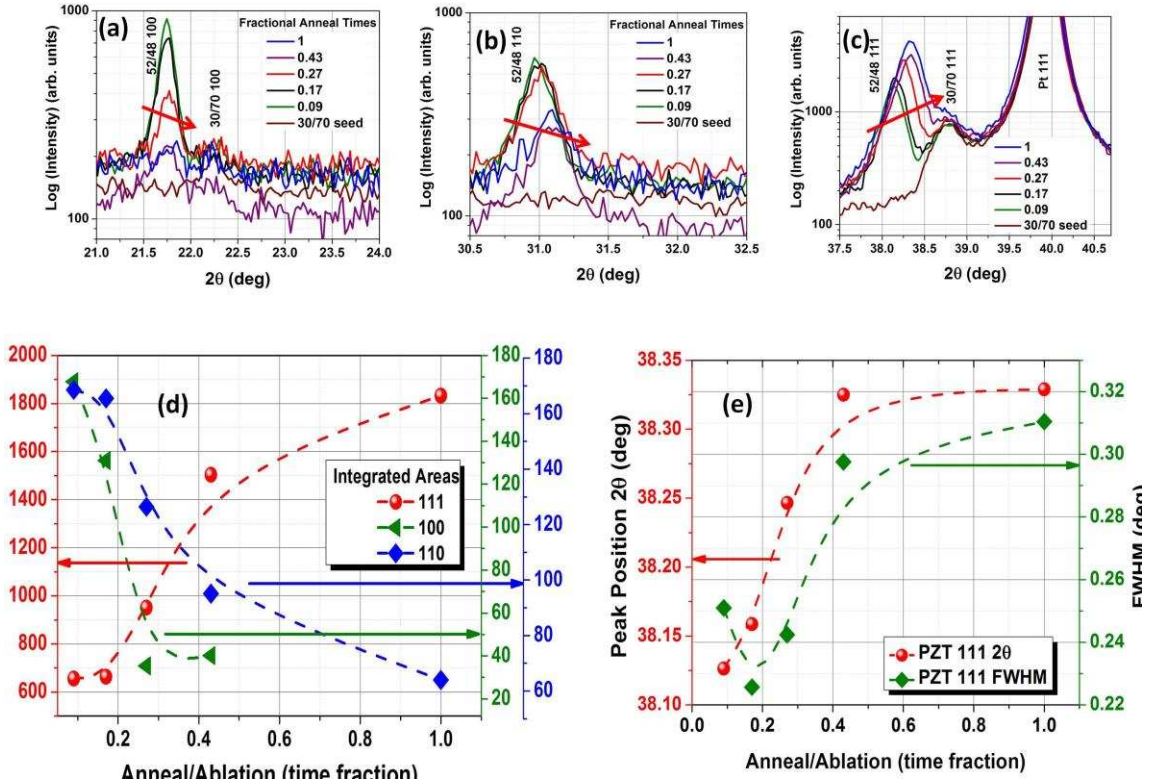

Figure 7: (a) 100_{pc}, (b) 110_{pc} and (c) 111_{pc} peaks with varying fractional laser anneals, (d) the integrated intensities and (e) 111 peak position and FWHM. The integrated intensities were calculated using the corresponding peak fits in Mathematica®.

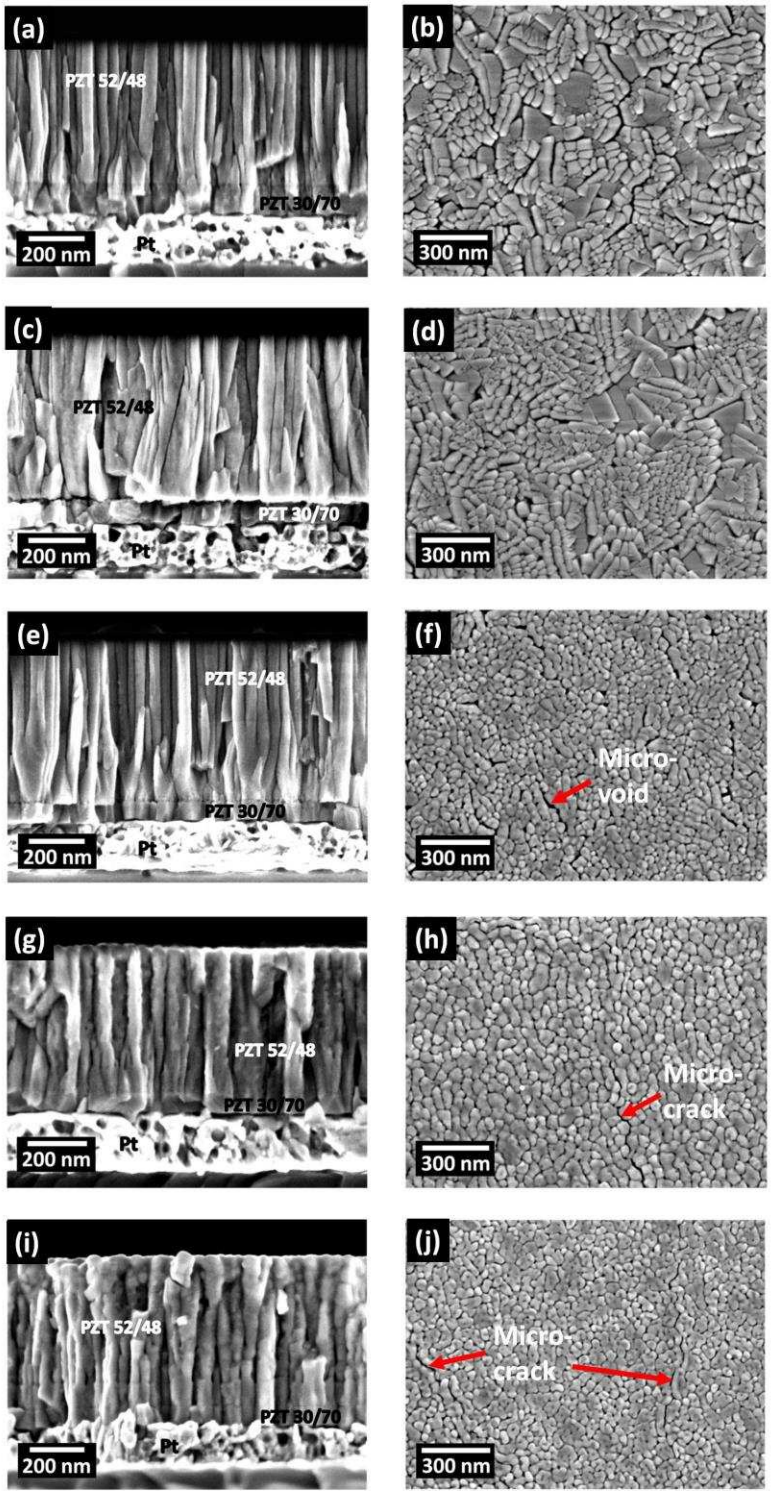

Figure 8: Microstructural changes as a function of fractional annealing time: 0.09 ((a) & (b)), 0.17 ((c) & (d)), 0.27 ((e) & (f)), 0.43 ((g) & (h)), 1 ((i) & (j)) (Micro-voids and micro-cracks have been labeled)

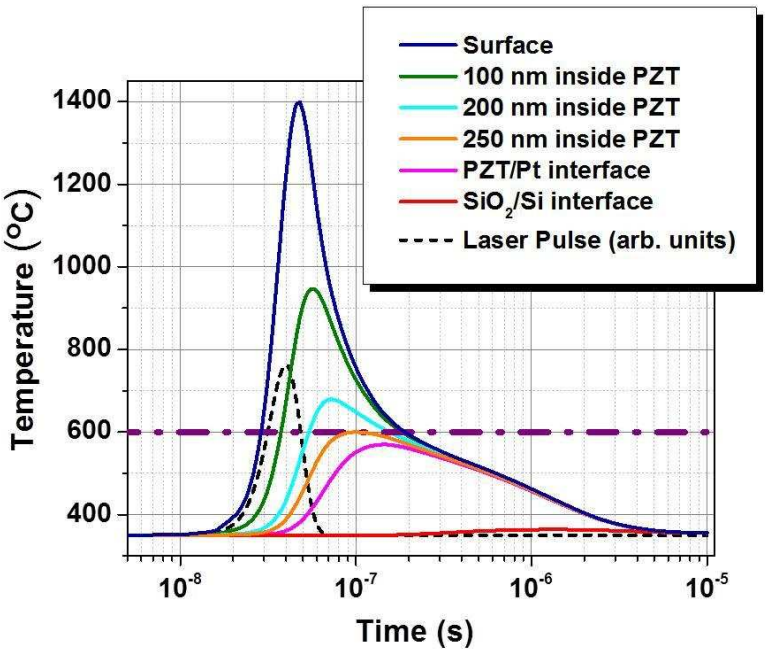

Figure 9: Temperature evolution at different depths inside 300 nm PZT on Pt/Ti/SiO_2/Si substrate. The laser pulse profile is also shown.

Table I: List of fractional anneal times investigated

Number of consecutive annealing pulses let in per shutter cycle	Number of blocked pulses on the annealing arm per shutter cycle	Number of consecutive deposition pulses per shutter cycle	Fractional Anneal Time (f_t^{Anneal})	Approximate number of cumulative annealing pulses for 590 nm PZT
3	0	3	3/3 (= 1)	~13074
3	4	7	3/7 (= 0.43)	~5622
3	8	11	3/11 (= 0.27)	~3530
3	15	18	3/18 (≈ 0.17)	~2223
3	30	33	3/33 (≈ 0.09)	~1177